Chapter 2

Application of Thin Piezoelectric Films in Diamond-Based Acoustoelectronic Devices

Boris P. Sorokin, Gennady M. Kvashnin, Andrey S. Novoselov, Sergey I. Burkov, Anton B. Shipilov, Nikolay V. Luparev, Victor V. Aksenenkov and Vladimir D. Blank

Additional information is available at the end of the chapter

http://dx.doi.org/10.5772/intechopen.76715

Abstract

The theory of external loading influence on acoustic parameters of piezoelectric five-layered structure as "Al/(001) AlN/Mo/(001) diamond/Me" has been developed. Oscillations in diamond-based high-overtone bulk acoustic resonators (HBARs) have been investigated in terms of 3D FEM simulation. Peculiarities of technology of aluminum-scandium nitride (ASN) films have been discussed. Composition $Al_{0.8}Sc_{0.2}N$ was obtained to create the diamond-based HBAR and SAW resonator. Application of ASN films has resulted in a drastic increasing an electromechanical coupling up to 2.5 times in comparison with aluminum nitride. Development of ASN technology in a way of producing a number of compositions with the better piezoelectric properties has a clear prospective. SAW resonator based on "Al IDT/(001) AlN/(001) diamond" structure has been investigated in the band 400–1500 MHz. The highest-quality factor $Q \approx 1050$ was observed for the Sezawa mode at 1412 MHz. Method of measuring HBAR's parameters within 4–400 K at 0.5–5 GHz has been developed. Results on temperature dependence of diamond's Q-factor at relatively low frequencies were quite different in comparison with the ones at the frequencies up to 5 GHz. Difference could be explained in terms of changing mechanism of acoustic attenuation from Akhiezer's type to the Landau-Rumer's one at higher frequencies in diamond.

Keywords: aluminum nitride, aluminum-scandium nitride, diamond-based HBAR, diamond-based SAW resonator, acoustoelectronic sensor, UHF

1. Introduction

Thin piezoelectric films (TPF) are the important components of many electronic sandwich devices due to its compatibility with the planar technology and comparatively low cost. Combination of effective TPF with non-piezoelectric substrate possessing the good acoustic properties allows obtaining the new micro devices especially in UHF bands. The matter is that the known single-crystalline piezoelectric materials as quartz, lithium niobate, tantalate, langasite, and langatate do not own a set of useful properties such as high electromechanical coupling, thermostable cuts, and good acoustic properties joined within a given crystal. Additionally, an enhancement of operational frequencies up to several GHz for bulk acoustic wave (BAW) resonators requires the thinning of crystal plates to the thickness close to several microns which seems really impossible because a lot of defects will be arisen. So, producing the best quality piezoelectric films compatible with any substrate materials is one of the main tasks of modern piezoelectric technology.

Since the end of the twentieth century, the zinc oxide (ZnO) and aluminum nitride (AlN) polycrystalline films with the wurtzite structure were widely used in such acoustoelectronic devices as composite resonators, filters, duplexers, etc. [1, 2]. It seems that the aluminum nitride has a more preferable combination of required qualities due to high dielectric properties as well as good temperature stability up to 1000 °C. First, in 2009 the authors [3] have found an enhancement of piezoelectric response in aluminum-scandium nitride (ASN) $Al_{1-x}Sc_xN$ solid solution. Therefore, aluminum-scandium nitride should be derived as prospective piezoelectric material for acoustoelectronic devices including sensors and energy harvesters. But the electromechanical properties of aluminum-scandium nitride are strongly depended on the scandium content, and as a result, its application in acoustoelectronic devices is discussible now.

High-overtone bulk acoustic resonator (HBAR) differs from conventional piezoelectric resonators due to their small size and high-quality factor Q at microwave operational frequencies [1]. A lot of materials have been successfully used to prepare the HBAR substrates: crystalline quartz, fused silica, silicon [4], sapphire [4, 5], and yttrium aluminum garnet (YAG) [6]. But the highest frequencies of the acoustic overtone excitation did not exceed 10 GHz. Recently, a distinctive progress in the achievement of record resonance frequencies up to 20 GHz has been emphasized by the development of HBAR based on piezoelectric layered structure (PLS) involving the single-crystalline diamond substrate and AlN thin-film piezoelectric transducer (TFPT) [7].

Naturally, thin piezoelectric films are widely used as the important elements in acoustoelectronic devices on surface acoustic waves (SAW), such as SAW delay lines, resonators, filters, and sensors. For example, in Ref. [8] the one-port SAW resonator, based on the layered structure AlN/polycrystalline diamond/Si and excited on the resonant frequency ~1.35 GHz, has been described. SAW filter at the frequency band ~6.3 GHz based on the structure SiO_2/AlN/polycrystalline diamond has been developed by authors [9].

A main aim of this paper was defined by the necessity in describing the modern trends in application of thin piezoelectric films as active elements in microwave acoustoelectronic

composite devices, including the choice and development of the new effective piezoelectric materials compatible with single-crystalline diamond substrates.

2. Theory of the thin-film loading influence on the acoustic parameters of diamond-based piezoelectric layered structure

An effective application of multilayered piezoelectric structure as a prototype of specialized acoustoelectronic sensor device should be based on the theory of the influence of an external loading on its acoustic parameters.

Propagation of the small amplitude acoustic waves of a piezoelectric crystal could be described basically by the equations of electrostatics and the equations of state of a piezoelectric medium written in coordinate form [10]:

$$\begin{aligned} \rho_0 \ddot{U}_i &= \tau_{ij,j}; \quad D_{m,m} = 0; \\ \tau_{ij} &= C^E_{ijkl}\eta_{kl} - e_{mij}E_m; \quad D_m = \varepsilon^{\eta}_{mn}E_n + e_{mij}\eta_{ij}, \end{aligned} \tag{1}$$

where ρ_0 is the density of a crystal, $\mathbf{U}_i$ is the vector of dynamic elastic displacements, τ_{ij} is the tensor of thermodynamic stresses, $\mathbf{D}_m$ is the vector of electrical induction, η_{kl} is the tensor of small deformations, C^E_{ijkl}, e_{mij}, and ε^{η}_{mn} are second-order elastic, piezoelectric, and clamped dielectric constants, respectively. The comma after the subscript denotes a spatial derivative, and coordinate Latin indices vary from 1 to 3. Here and further, the rule of summation over repeated indices will be used. For elastic displacements and the electric potential in the form of small-amplitude plane monochromatic waves, the system of equations was written in the form of the well-known Green-Christoffel equations, which must be solved for each layered medium to be used:

$$\begin{aligned} &\left(\Gamma_{ik} - \rho_0\omega^2\delta_{ik}\right)\alpha_i = 0; \qquad i,k = 1\ldots4; \qquad \delta_{44} = 0; \\ &\Gamma_{ik} = C_{ijkm}k_jk_m; \ \Gamma_{4j} = \Gamma_{j4} = e_{ijk}k_ik_k; \ \Gamma_{44} = -\varepsilon^{\eta}_{nm}k_nk_m \end{aligned} \tag{2}$$

where $\vec{k} = \frac{\omega}{V}\vec{n}$ is the wave vector; $\vec{n}$ is the unit vector of wave propagation; ω and V are the angular frequency and phase velocity of an elastic wave, respectively; α_i is the component of eigenvectors of elastic displacement; and α_4 is the amplitude of the wave of quasistatic electrical potential connected with an elastic wave. Solving of Green-Christoffel equations taken in a general form, Eq. (2) allows to define the parameters of propagation both the bulk and surface acoustic waves in piezoelectric layered structure.

Let the X_3 axis of operational coordinate system be directed along the outer normal to the surface of the layer, and the X_1 axis coincides with the wave propagation direction (**Figure 1**). In a multilayer piezoelectric structure, describing the propagation of the elastic waves, it is necessary to write down the special boundary conditions, which, depending on the number m of layers, take a form:

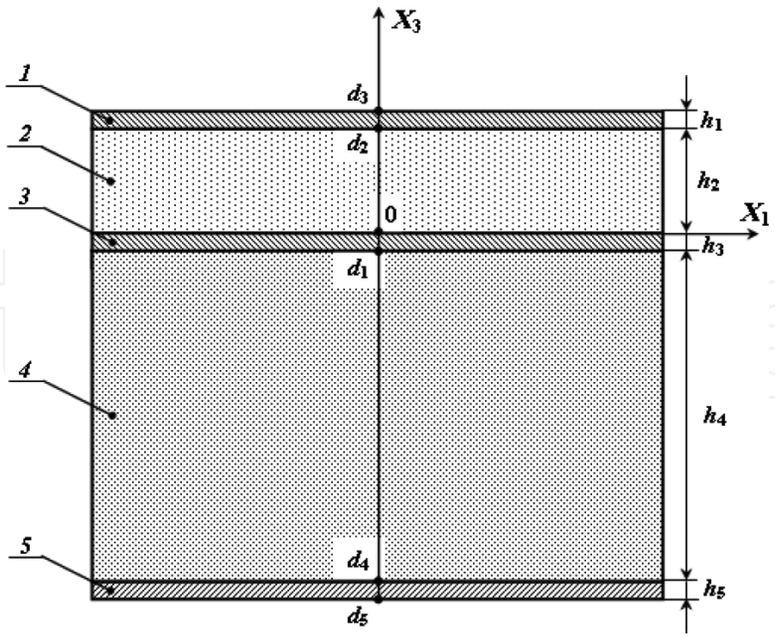

Figure 1. Arrangement of a piezoelectric layered structure: (*1*) top electrode, (*2*) piezoelectric film, (*3*) bottom electrode, (*4*) substrate, and (*5*) the layer to be investigated.

$$
\begin{aligned}
&\tau_{3i}^{(1)} = 0\Big|_{x_3=h_1}, \quad D_3^{(1)} = D^{(\text{вак})}\Big|_{x_3=h_1};\\
&\tau_{3i}^{(1)} = \tau_{3i}^{(2)}\Big|_{x_3=h_2}, \quad D_3^{(1)} = D_3^{(2)}\Big|_{x_3=h_2}; \varphi^{(1)} = \varphi^{(2)}\big|_{x_3=h_2}; \quad U_i^{(1)} = U_i^{(2)}\Big|_{x_3=h_2};\\
&\cdots\cdots\cdots\\
&\tau_{3i}^{(m-1)} = \tau_{3i}^{(m)}\Big|_{x_3=0}, \quad D_3^{(\text{m}-1)} = D_3^{(m)}\Big|_{x_3=0}; \varphi^{(m-1)} = \varphi^{(m)}\big|_{x_3=0}; \quad U_i^{(m-1)} = U_i^{(m)}\Big|_{x_3=0};\\
&\tau_{3i}^{(m)} = 0\Big|_{x_3=-h_n}, \quad D_3^{(m)} = D^{(\text{вак})}\Big|_{x_3=-h_m}.
\end{aligned}
\tag{3}
$$

Here, h_1, …, h_m are the layer thicknesses. Substituting into boundary conditions (3) the required solutions as a linear combinations of the partial waves

$$
\begin{aligned}
U_i^{(m)} &= \sum_n C_n^{(m)} \alpha_i^{(n)} \exp\left[i\left(k_1 x_1 + k_3{}^{(n)} x_3 - \omega t\right)\right],\\
\Phi^{(m)} &= \sum_n C_4^{(m)} \alpha_4^{(n)} \exp\left[i\left(k_1 x_1 + k_3{}^{(n)} x_3 - \omega t\right)\right],
\end{aligned}
\tag{4}
$$

one can obtain a matrix of boundary conditions, and the vanishing of its determinant allows obtaining the equations for determining the parameters of elastic wave propagation. In Eq. (4) a superscript n is associated with nth partial wave. By varying the boundary conditions (Eq. (3)), one can specify all the types of PLS elastic waves. For example, the first equation in Eq. (3) is related to the Rayleigh-type SAW propagation. The first and last equations together describe the propagation of Lamb-type elastic waves in a piezoelectric plate with a thickness h, i.e., in this case Eq. (3) at m = 1. taking the form

$$\begin{cases} \sum_{n=1}^{8} C_n \left[C_{3jkm} k_m^{(n)} \alpha_k^{(n)} + e_{k3j} k_k^{(n)} \alpha_4^{(n)} \right] \exp\left[i k_3^{(n)} h \right] = 0; \\ \sum_{n=1}^{8} C_n \left[e_{3km} k_m^{(n)} \alpha_k^{(n)} - \left(\varepsilon_{3k} k_k^{(n)} - i\varepsilon_0 \right) \alpha_4^{(n)} \right] \exp\left[i k_3^{(n)} h \right] = 0; \\ \sum_{n=1}^{8} C_n \left[C_{3jkm} k_m^{(n)} \alpha_k^{(n)} + e_{k3j} k_k^{(n)} \alpha_4^{(n)} \right] = 0; \\ \sum_{n=1}^{8} C_n \left[e_{3km} k_m^{(n)} \alpha_k^{(n)} - \left(\varepsilon_{3k} k_k^{(n)} + i\varepsilon_0 \right) \alpha_4^{(n)} \right] = 0. \end{cases} \tag{5}$$

At the assumption that the lower layer is sufficiently thick (semi-infinite), i.e., the thickness of a layer should be much greater than the length of the elastic wave, in which case the last equation in Eq. (3) cannot be taken into account, i.e., the presence of a free lower boundary will be ignored. It is also necessary to require that the condition $\mathrm{Im}\left(k_3{}^{(m)}\right) < 0$ ensuring the attenuation of the elastic wave into the depth of a substrate should be satisfied. Thus, the boundary conditions (Eq. (3)) describing the elastic wave propagation in the "layer-substrate" structure will have the form.

$$\begin{aligned} &\sum_{n=1}^{8} \left[a_n C_{3kpi}^{(1)} k_i^{(n)} \alpha_p^{(n)} + a_4 e_{p3k}^{(1)} k_p^{(n)} \alpha_4^{(n)} \right] \exp\left[i k_3^{(n)} h \right] = 0, \\ &\sum_{n=1}^{8} \left[a_n e_{3kl}^{(1)} k_l^{(n)} \alpha_k^{(n)} + a_4 \left(\varepsilon_{3k}^{(1)} k_k^{(n)} - i\varepsilon_0 \right) \alpha_4^{(n)} \right] \exp\left[i k_3^{(n)} h \right] = 0, \\ &\sum_{m=1}^{4} b_m \left[C_{i3kl}^{(2)} k_l^{(s)} \alpha_k^{(s)} + e_{3pi}^{(2)} k_p^{(s)} \alpha_4^{(s)} \right] - \sum_{n=1}^{8} a_n \left[C_{i3kl}^{(1)} k_l^{(n)} \alpha_k^{(n)} + e_{3pi}^{(1)} k_p^{(n)} \alpha_4^{(n)} \right] = 0, \\ &\sum_{m=1}^{4} b_m \left[e_{3kl}^{(2)} k_l^{(s)} \alpha_k^{(s)} + \varepsilon_{3k}^{(2)} k_k^{(s)} \alpha_4^{(s)} \right] - \sum_{n=1}^{8} a_n \left[e_{3kl}^{(1)} k_l^{(n)} \alpha_k^{(n)} + \varepsilon_{3k}^{(1)} k_k^{(n)} \alpha_4^{(n)} \right] = 0, \\ &\sum_{s=1}^{4} U_i^{(2)(s)} b_m - \sum_{n=1}^{8} U_i^{(1)(n)} a_n = 0. \end{aligned} \tag{6}$$

Here, the digital superscripts 1 and 2 denote the layer and the substrate, respectively; $\alpha_k^{(s)}$ and b_m are the amplitude and weight coefficients of the mth partial wave (m = 1, …, 4) in a substrate; and $\alpha_k^{(n)}$ and a_n are the amplitude and weight coefficients of the nth partial wave (n = 1, …, 8) in a piezoelectric layer.

In modern acoustoelectronics, accurate information about the mechanical parameters of thin layers of new materials and thin mono- and polycrystalline films used to create microwave acoustic resonators, filters, and sensors should be of great importance. Previously proposed and used in a number of experiments, the original method of resonance acoustic microwave spectroscopy has opened a possibility of measuring these parameters [11]. The essence of such method was based on the investigated film that was included into a content of an acoustic

composite microwave resonator changing its acoustic parameters (**Figure 1**). Connection with the external electrical circuit was carried out by the TFPT. In the case of thin films, the last one should be deposited on a sufficiently thick substrate made of a material with low acoustic losses. Information on the attenuation coefficient and sound velocity in the film were found from the comparison of the measured total losses and the positions of the resonant peaks without the film and after its deposition.

To solve the problems of acoustic microwave spectroscopy, it is necessary to introduce a system of boundary conditions for the PLS according to **Figure 1**. For elastic displacements in the form of a plane sinusoidal wave, one can be written as

$$U^{(S)} = a^{(S)}\exp\left(-ik^{(S)}x_3\right) + b^{(S)}\exp\left(ik^{(S)}x_3\right), \tag{7}$$

where the subscript S denotes the medium used in calculations; $a^{(S)}$ and $b^{(S)}$ are the amplitudes of the incident and reflected elastic waves in the Sth layer, respectively; and k is the modulus of the wave vector in a layer.

Assuming that the electrodes were consisted of isotropic metals, the piezoelectric layer had the crystalline symmetry as 6 *mm*, the substrate was taken as a cubic dielectric crystal, and the layer to be investigated was isotropic, the boundary conditions have been formulated as follows:

(1) Stress tensor should have the zero normal components at the interface "top electrode-vacuum" in the form

$$\tau_{3j}^{(1)} = 0\Big|_{x_3=d_3} = -a^{(1)}k^{(1)}C^{(1)}\exp\left(-ik^{(1)}d_3\right) + b^{(1)}k^{(1)}C^{(1)}\exp\left(ik^{(1)}d_3\right) = 0, \tag{8}$$

where $k^{(1)}$ is the wave vector at the top electrode layer, $C^{(1)} = C_{11}$ is the elastic modulus of the top electrode film *1*, and d_3 is the point on the interface "top electrode-vacuum." Here and after the superscript designates the PLS layer's number.

(2) Normal components of the stress tensor and displacement vectors should be equal to appropriate values taken at the interface "top electrode-piezoelectric film" as follows:

$$\begin{aligned}
&\tau_{3j}^{(1)} = \tau_{3j}^{(2)}\Big|_{x_3=d_2}, \quad U^{(1)} = U^{(2)},\\
&-a^{(1)}k^{(1)}C^{(1)}\exp\left(-ik^{(1)}d_2\right) + b^{(1)}k^{(1)}C^{(1)}\exp\left(ik^{(1)}d_2\right) - a^{(2)}k^{(2)}C^{(2)}P - b^{(2)}k^{(2)}C^{(2)}P^* = e\frac{V_0}{h_2},\\
&P = \exp\left(-ik^{(2)}d_2\right) + \frac{ie^2}{\varepsilon C^{(2)}k^{(2)}d_2}\left[\exp\left(ik^{(2)}d_2\right) - 1\right],\\
&a^{(1)}\exp\left(-ik^{(1)}d_2\right) + b^{(1)}\exp\left(ik^{(1)}d_2\right) - a^{(2)}\exp\left(-ik^{(2)}d_2\right) - b^{(2)}\exp\left(ik^{(2)}d_2\right) = 0.
\end{aligned} \tag{9}$$

In Eq. (9) the following notations are introduced: P^* is a complex conjugated value; $C^{(2)} = C_{33}$, $e = e_{33}$, and $k^{(2)}$ are the elastic modulus, the piezoelectric constant, and the wave vector in piezoelectric film *2*, respectively; d_2 is the point on the interface "top electrode-piezoelectric

film"; $U^{(2)}$ and $U^{(1)}$ are the elastic displacement vectors in piezoelectric layer and top electrode, respectively; V_0 is the potential difference between the electrodes; h_2 is the thickness of piezoelectric layer.

(3) Normal components of the stress tensor and displacement vectors should be equal to appropriate values taken at the interface "piezoelectric film-bottom electrode" as follows:

$$\begin{aligned} &\tau_{3j}^{(2)} = \tau_{3j}^{(3)}\Big|_{x_3=0}, \quad U^{(2)} = U^{(3)}, \\ &a^{(3)}k^{(3)}C^{(3)} + b^{(3)}k^{(3)}C^{(3)} + a^{(2)}k^{(2)}C^{(2)} - b^{(2)}k^{(2)}C^{(2)} = e\frac{V_0}{h_2}, \\ &a^{(3)} + b^{(3)} - a^{(2)} - b^{(2)} = 0. \end{aligned} \tag{10}$$

In Eq. (10) the following notations are introduced: $C^{(3)} = C_{11}$, $U^{(3)}$, and $k^{(3)}$ are the elastic modulus, the elastic displacement, and the wave vector in the bottom electrode *3*, respectively.

(4) Normal components of the stress tensor and displacement vectors should be equal to appropriate values taken at the interface "bottom electrode-substrate" as follows:

$$\begin{aligned} &\tau_{3j}^{(4)} = \tau_{3j}^{(3)}\Big|_{x_3=d_1}, U^{(4)} = U^{(3)}, \\ &a^{(3)}k^{(3)}C^{(3)}\exp\left(ik^{(3)}d_1\right) - b^{(3)}k^{(3)}C^{(3)}\exp\left(-ik^{(3)}d_1\right) - a^{(4)}k^{(4)}C^{(4)}\exp\left(ik^{(4)}d_1\right) - b^{(4)}k^{(4)}C^{(4)}\exp\left(-ik^{(4)}d_1\right) = 0, \\ &a^{(3)}\exp\left(ik^{(3)}d_1\right) + b^{(3)}\exp\left(-ik^{(3)}d_1\right) - a^{(4)}\exp\left(ik^{(4)}d_1\right) - b^{(4)}\exp\left(-ik^{(4)}d_1\right) = 0. \end{aligned} \tag{11}$$

In Eq. (11) the following notations are introduced: $C^{(4)} = C_{11}$, $U^{(4)}$, and $k^{(4)}$ are the elastic modulus, the elastic displacement, and the wave vector in the substrate *4*, respectively, and d_1 is the point on the interface "bottom electrode-substrate."

(5) Normal components of the stress tensor and displacement vectors should be equal to appropriate values taken at the interface "substrate-the layer to be investigated" as follows:

$$\begin{aligned} &\tau_{3j}^{(4)} = \tau_{3j}^{(5)}\Big|_{x_3=d_4}, \ U^{(4)} = U^{(5)}, \\ &a^{(5)}k^{(5)}C^{(5)}\exp\left(ik^{(5)}d_4\right) - b^{(5)}k^{(5)}C^{(5)}\exp\left(-ik^{(5)}d_4\right) - a^{(4)}k^{(4)}C^{(4)}\exp\left(ik^{(4)}d_4\right) + b^{(4)}k^{(4)}C^{(4)}\exp\left(-ik^{(4)}d_4\right) = 0, \\ &a^{(5)}\exp\left(ik^{(5)}d_4\right) + b^{(5)}\exp\left(-ik^{(5)}d_4\right) - a^{(4)}\exp\left(ik^{(4)}d_4\right) - b^{(4)}\exp\left(-ik^{(4)}d_4\right) = 0. \end{aligned} \tag{12}$$

In Eq. (12) the following notations are introduced: $C^{(5)} = C_{11}$, $U^{(5)}$, and $k^{(5)}$ are the elastic modulus, the elastic displacement, and the wave vector in the layer *5*, respectively, and d_4 is the point on the interface "substrate-the layer to be investigated."

(6) Normal components of the stress tensor should be equal to appropriate values taken at the "the layer to be investigated-vacuum" as follows:

$$\begin{aligned} &\tau_{3j}^{(5)} = 0\Big|_{x_3=d_5}, \\ &a^{(5)}k^{(5)}C^{(5)}\exp\left(ik^{(5)}d_5\right) - b^{(5)}k^{(5)}C^{(5)}\exp\left(-ik^{(5)}d_5\right) = 0, \end{aligned} \tag{13}$$

where d_5 is the point on the interface "the layer to be investigated-vacuum."

Boundary conditions (Eq. (8)–(13)) form a system of equations as 10×10 dimensions, the solution of which makes it possible to determine the amplitudes of the elastic waves in all the layers and the PLS frequency characteristics. Note that the part of the boundary condition matrix as 7×7 dimensions allows to obtain the so-called form factor of HBAR including into calculation a traveling acoustic wave only, i.e., without taking into account the lower boundary of the crystalline substrate (12) and (13). Additionally, when Eq. (12) was taken into account, as a result appropriate boundary condition matrix as 8×8 dimensions can be formed, and the HBAR's form factor can be calculated including the influence of a bottom boundary of a substrate.

In order to study the influence of the fifth layer on the PLS acoustic parameters, a required own software "Modeling of the processes of resonant acoustic spectroscopy in multilayered structures" based on the above theory has been developed [12]. An estimation of the influence of metal film deposition as a fifth layer on the change of the overtone resonant frequency of diamond-based PLS "Al/(001) AlN/Mo/(001) diamond/Al (Mo)" is presented in **Figure 2**. In calculations the thickness of Al or Mo films was varied within 0–1300 nm. As one can see, the metal deposition leads to the decrease of resonant frequency with the thickness increasing both the metals. But on the curve associated with Al influence, the sharp variation of resonant frequency in the vicinity of 400–600 nm takes place on the contrary with the linearly

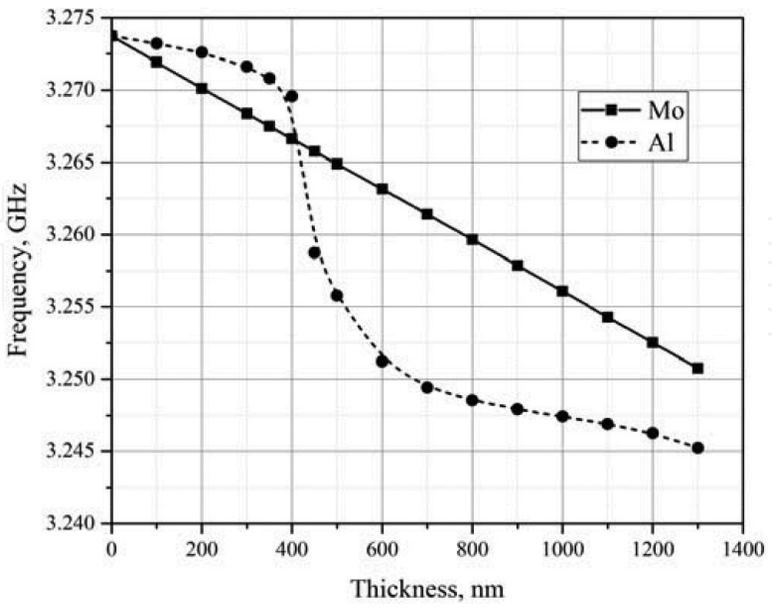

Figure 2. Change in an overtone resonant frequency of diamond-based PLS by metal film deposition. In calculation the PLS "Al/(001) AlN/Mo/(001) diamond/Al (Mo)" was used with thicknesses (in microns) of the films and substrate as "0.14/1.125/0.16/501/0–1.2," respectively.

http://dx.doi.org/10.5772/intechopen.76715

proportional dependence of resonant frequency on the thickness of Mo film. This can be explained by the quite different acoustic impedances $Z = \rho V$ of Al and Mo as 17 and 63 (in 10^6 kg/s·m^2), respectively. As a result, the elastic waves falling from the substrate on the diamond-Al or diamond-Mo boundaries should be mainly reflected or should pass through the boundary freely, respectively. But because the quarter-wave, thickness in the Al layer is approximately equal to 450 nm at 3.26 GHz; in this case the Al film should become an antireflective one, which leads to a sharp increase in the effective thickness of the substrate and, correspondingly, to a stepwise decrease in the resonant frequency. On the other hand, a monotonic increase in the Mo film thickness leads only to a smooth increase in the effective thickness of the substrate and, correspondingly, to a linearly proportional decrease of the resonant frequency.

3. 3D simulation of acoustic wave propagation in multilayered piezoelectric structure

Earlier [13, 14], we have successfully applied the 2D FEM simulation in order to obtain a quite complex pattern of dispersive dependences of phase velocities of plate Lamb waves observing visualization of the fields of elastic displacements belonging to a lot of acoustic modes with a number of eigenfrequencies. Besides of Lamb waves, the BAW and SAW modes of Rayleigh type were found. But the statement of the task in 2D approximation did not allow obtaining the results on the SH modes.

In the 3D FEM simulation as a model, the PLS "Al/(001) AlN/Mo/(001) diamond" has been investigated by the software COMSOL Multiphysics. Boundary conditions on the top and bottom surfaces of a model sample were chosen as the free ones, and on all the vertical surfaces as the symmetrical ones. Width×length×thickness (in microns) of diamond substrate and AlN film were 1000×1000×392 and 400×400×0.624, respectively. Thicknesses (in nm) of Al and Mo films were taken as 164 and 169, respectively. All the dimensions of a model sample were close to appropriate ones in the experimental sample. In **Figure 3**, the results on the second overtone of longitudinal bulk acoustic wave in the PLS investigated are presented as 2D and 3D images. Note

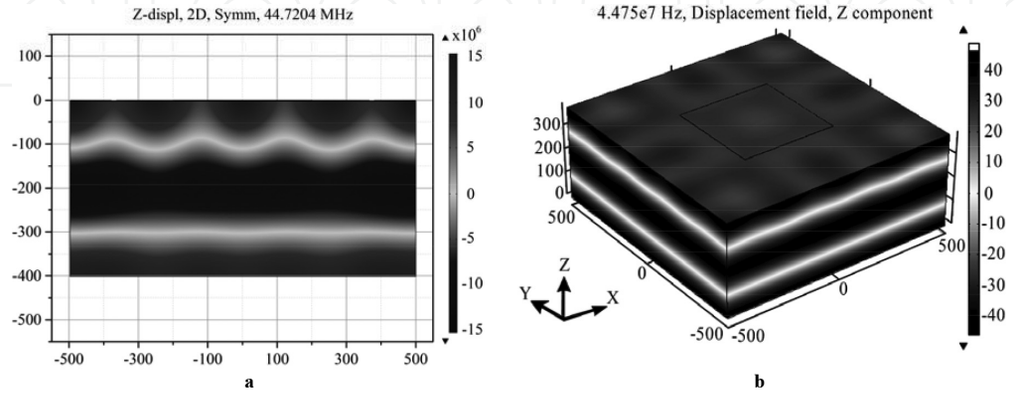

Figure 3. Elastic displacement fields (Z-component) within a model PLS in 2D (a) and 3D (b) approximation for longitudinal bulk acoustic wave propagating along Z-axis.

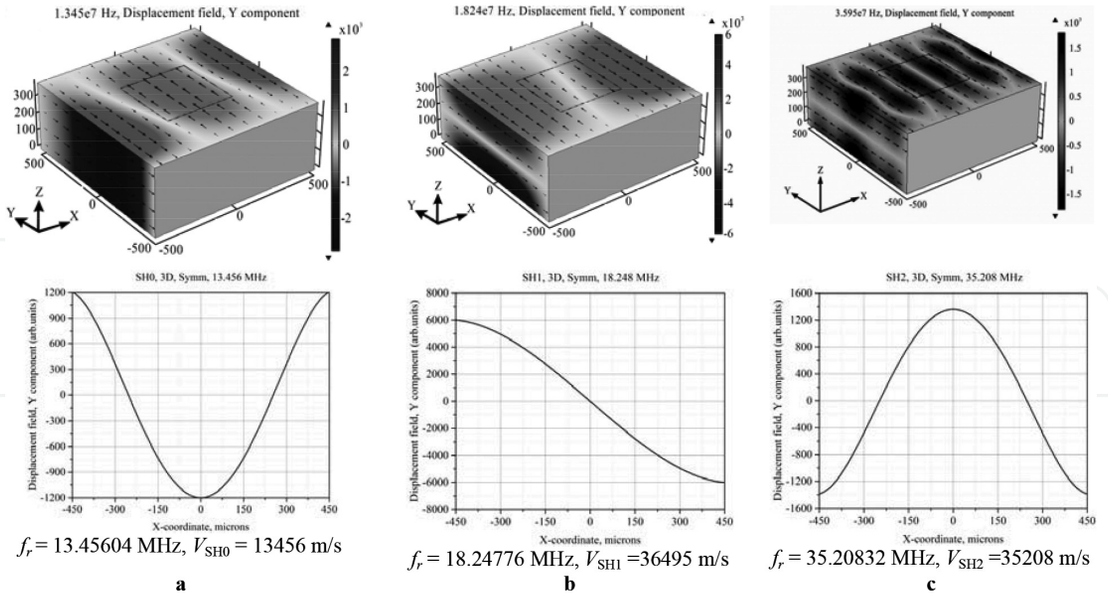

Figure 4. Elastic displacement fields (Y-component) within a model PLS in 3D approximation for SH_0 (a), SH_1 (b), and SH_2 (c) dispersive modes. Arrows should be associated with the vectors of a local elastic displacement.

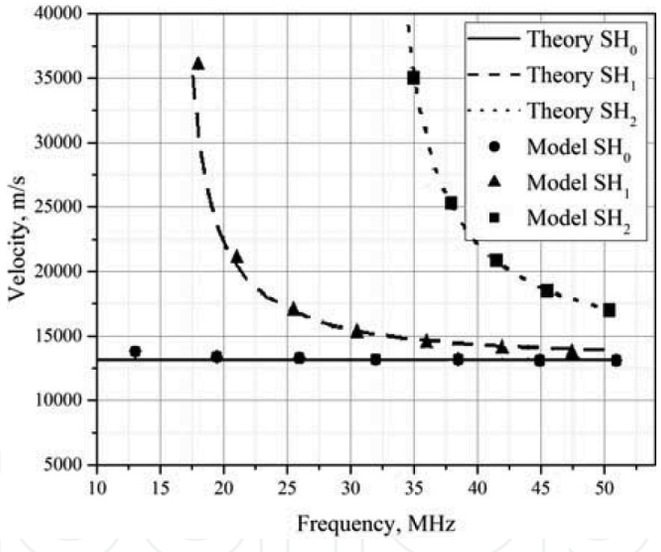

Figure 5. Dependences of SH-type wave velocities on the frequency for the SH_0, SH_1, and SH_2 dispersive branches in the PLS "Al/(001) AlN/Mo/(001) diamond" in comparison with theory data.

that the calculated data on resonant frequency (in MHz) as 44.72 obtained in 2D approximation (**Figure 3a**) are in close accordance with the similar as 44.75 (**Figure 3b**) in 3D approximation.

In **Figure 4**, an example of the data on the elastic displacement patterns arising for the SH-type waves in the PLS "Al/(001) AlN/Mo/(001) diamond" is presented in 3D image. SH waves are dispersive and deeply penetrating into a substrate. As a consequence, SH wave velocities should be strongly depended on the operational frequency. Such dependences for a number of first

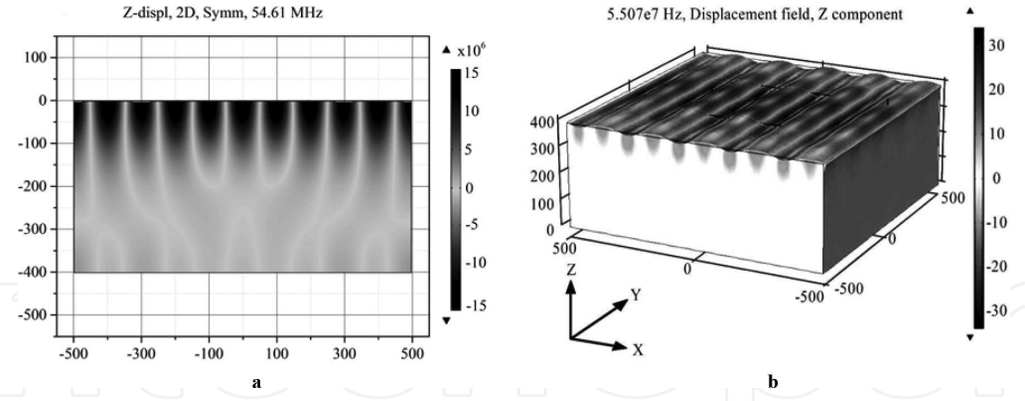

Figure 6. Z-components of elastic displacement fields within a model PLS "Al/(001) AlN/Mo/(001) diamond" in 2D (a) and 3D (b) approximation for Rayleigh-type surface wave propagating along X-axis.

dispersive branches within the frequency band 10–50 MHz are presented in **Figure 5** in comparison with theory data. As one can see, a good agreement between the model and theory was obtained.

In **Figure 6** an example of the elastic displacement patterns arising for the Rayleigh-type waves in the PLS "Al/(001) AlN/Mo/(001) diamond" is presented in 2D and 3D image. As one can calculate, the SAW wave lengths in a diamond were both equal to 200 microns in 2D and 3D approximation, and the SAW phase velocities were equal to 10,922 and 11,014 m/s, respectively. One can speak about a reasonable agreement between the results of two models.

4. Aluminum nitride and aluminum-scandium nitride film preparation: sample characterization

In our microwave experiments, a lot of devices under test (DUT) operating the BAW or SAW propagation in PLS were required (**Figure 7**). As one can see, it was necessary to fabricate the

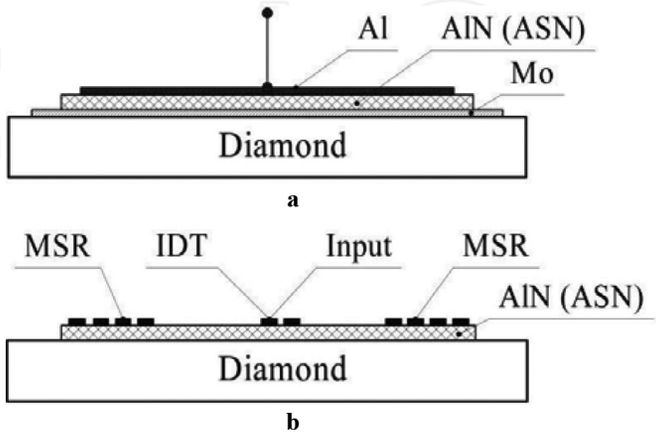

Figure 7. Devices under test. (a) BAW resonator based on the PLS "Al/AlN or ASN piezoelectric film/Mo/diamond" and (b) single-port SAW resonator based on the PLS "Al IDT/AlN or ASN piezoelectric film/diamond." IDT and MSR are the interdigital transducer and microstrip reflector, respectively.

multilayered piezoelectric structures involving the TFPT and diamond substrate (**Figure 7a)** or IDT/AlN (ASN) piezoelectric film on diamond substrate (**Figure 7b)**. Here, IDT is an interdigital transducer conventionally applied in a number of SAW devices to SAW exciting and detection.

The IIa type synthetic diamond single crystals grown by HPHT method at the Technological Institute for Superhard and Novel Carbon Materials were used as substrates for producing in all the DUTs investigated. Such crystals have the good dielectric properties and a low content of nitrogen impurity. All the substrates with the orientation of the main surfaces (100), (110), and (111) were double side polished up to roughness R_a within 0.2–2 nm on 10×10 μm^2 area controlled by AFM method. As a result of the mechanical grinding and polishing, roughness and a buried damage layer (BDL) underneath the crystalline surface should take place. In order to control the BDL depth, we applied the method of electron backscatter diffraction (EBSD) and Kikuchi line (KL) observation [15]. Appearance of clear KL is closely correlated with the BDL absence. As a summary, one can highlight the unique peculiarity of single-crystalline diamond: multiple EBSD experiments involving the faces with different treatment degrees, as well as natural faces of as-grown crystal, have produced practically the same clear KL patterns. So, the BDL depth of the diamond substrate can be estimated as several atomic layers. This fact was first discovered by us and drastically singles out crystalline diamond from the set of any other conventionally applications in acoustoelectronic device materials. As a result, the BDL can only have a weak influence on the UHF acoustic properties of diamond.

Metal electrodes, aluminum nitride or aluminum-scandium nitride piezoelectric films, were deposited by magnetron sputtering equipment AJA ORION 8. Process of aluminum-scandium nitride synthesis in comparison with that for AlN was differed by the application of additional Sc target, so the Al and Sc targets were in work simultaneously. One can see from the available experimental data [16] that a significant increase in piezoelectric module d_{33} (more than in four times) in solid solution $Al_{1-x}Sc_xN$ has took place with increasing scandium concentration. On the other hand, pure scandium nitride (ScN) should belong to a cubic symmetry with the centrosymmetrical space group F*m*3*m* and the rock salt structure (*rs*), which leads to an absence of piezoelectricity. It was shown [16] that the hexagonal piezoelectric structure of wurtzite type (*wz*) has been stably existed within $0 \le x \le 0.43$ only. Coexistence of *wz* and *rs* phases should be observed at $0.43 \le x \le 0.55$, while the *rs* structure was preferably observed when $0.55 < x \le 1.0$. So, a required Sc concentration leading to the maximal piezoelectric properties in the solid solution $Al_{1-x}Sc_xN$ should be exactly equal to $x = 0.43$. But in practice an exact equality could be hardly obtained. In the aim of our experiment, the content of gas mixture N_2/Ar as well as other synthesis parameters was chosen to obtain the $Al_{0.8}Sc_{0.2}N$ composition. One can see by the X-ray diffraction pattern for the test sample ASN/Mo/glass (**Figure 8**) that the ASN film has the preferred orientation (00·2) and the full width at half maximum for this reflection is 0.24°. This shows a good quality texture of axial type along the sixfold axis of the wurtzite-type structure. The X-ray diffraction measurements were performed by Empyrean PANalytical equipment.

A preferred choice of Mo as a bottom electrode was explained by a good accordance between acoustical impedances of diamond substrate and Mo. Aluminum chosen as a material of top

http://dx.doi.org/10.5772/intechopen.76715

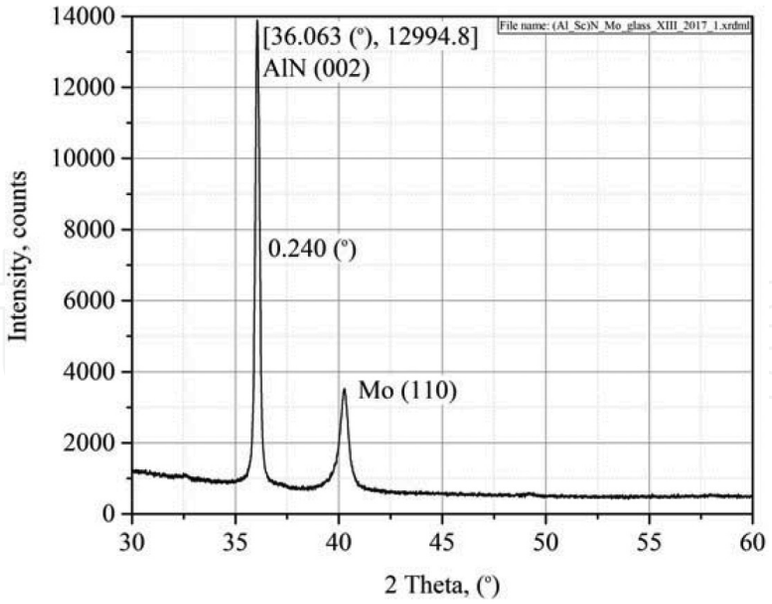

Figure 8. The X-ray diffraction pattern for the test sample ASN/Mo/glass.

electrode can be described as the metal with good conductance and low density. The last property is useful because the deposition of top electrode should be influenced on PLS properties as less as possible. Electrode structures with a specified topology were deposited using photolithography process by the Heidelberg μPG 101 equipment. Explosive photolithography process was necessary to form a specified AlN or ASN film topology. Increasing an accuracy of IDT manufacturing and other electrode structures was connected with an understanding of the physical and chemical features of photolithography process in application to the small-sized substrates. Since the deposition of Al electrodes in the PLS investigated was performed on the surface of AlN or ASN piezoelectric films, it should be taken into account that their surfaces had a distinctive relief defined by triangular pyramid tops of crystallites, so that the roughness of such surfaces can be about 20–30 nm. Deposited Al films should overlap these irregularities. The thickness of deposed metal films was varied within 150–200 nm for the top electrode and 150–200 nm for the bottom one.

5. Microwave investigation tools and measurement methods

Method of low-temperature (LT) microwave studies of PLS acoustic properties was developed on the vector network analyzer E5071C-2 K5 (300 kHz–20 GHz), the probe station M150, the automated low-temperature system for measuring material properties Quantum Design Physical Property Measurement System EverCool II (4–400 K), and the nonstandard LT adapter (**Figure 9**).

To carry out the microwave measurements with HBARs as experimental samples, due to a weak level of the useful signal against the noise, and to obtain the correct quantitative value of the impedance, it must calibrate the whole measuring circuit consisting of a probe, a microwave cable, and a vector network analyzer. Typically, this procedure is performed near the

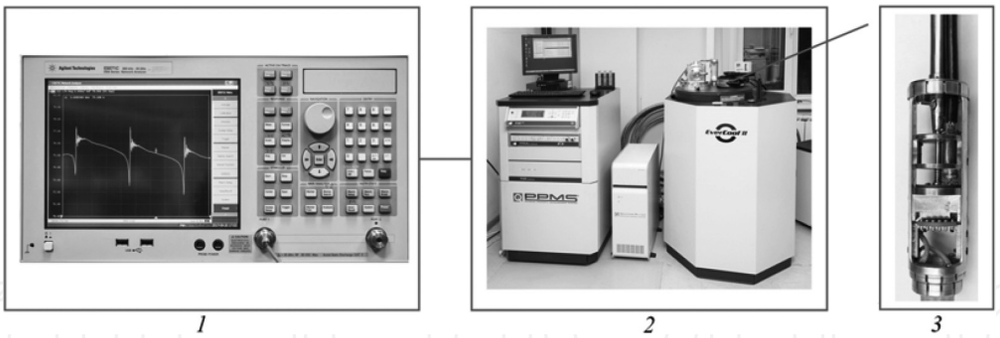

Figure 9. Block diagram of low-temperature microwave measurements: (*1*) vector network analyzer E5071C, (*2*) cryogenic control and temperature stabilization system Quantum Design PPMS EverCool II, and (*3*) LT measuring adapter.

room temperature at the probe station using a special calibration plate. However, for cryogenic temperatures, the use of a probe station was impossible. We have developed the LT measuring adapter that made possible to measure the complex reflection coefficient $\widehat{S}_{11}(f)$ of microwave signal obtained by HBAR conjugated with the possibility of calibration procedure starting from cryogenic temperatures up to 400 K.

Since all measurements were carried out using a reflected signal, a single-port connection scheme with open-short-load calibration options was selected for measurement and calibration. The calibration elements corresponding to these options were located on the operational disk made of corundum ceramics with contact pads from Au/Pt/Ti produced by the photolithography method. Connection of a measured sample to the contact pads on the operational disk was done by adhering with a silver paste SPI 5001-AB Silver Paint, resistant to both low and high temperatures. At the same time, two measured samples could be placed on the operational disk. Control measurements on the same sample, carried out at room temperature by M150 probe station or using a low-temperature measuring adapter, were in a good agreement.

The method for measuring the sound phase velocity in a substrate was based on the determination of the HBAR's eigenfrequencies taking into account the frequency and temperature dependences of the complex reflection coefficient $\widehat{S}_{11}(f)$ in the composite resonator. Then, the complex impedance $\widehat{Z}_{11}(f)$ of the measuring circuit along with the sample was calculated with the help of vector analyzer software in accordance with the relation:

$$\widehat{Z}_{11}(f) = Z_0 \frac{1+\widehat{S}_{11}(f)}{1-\widehat{S}_{11}}(f), \tag{14}$$

where Z_0 is the input impedance of the microwave circuit equal to 50 Ω. The full impedance $\widehat{Z}_{11}(f)$ included the quantity $\widehat{Z}_{11t}$ of the microwave cable together with the contacts and HBAR's "pure" impedance $\widehat{Z}_{11e}$ as

$$\widehat{Z}_{11}(f) = \widehat{Z}_{11t}(f) + \widehat{Z}_{11e}(f). \tag{15}$$

Required impedance $\widehat{Z}_{11e}(f)$ was determined by Eq. (15) where the value $\widehat{Z}_{11t}$ was experimentally determined at the frequency outside the resonance one of the given overtones. Taking the

$\widehat{Z}_{11e}(f)$ values by the vector analyzer software, the frequency dependence of HBAR's loaded quality factor $Q(f)$ was calculated at a − 3 dB level about the maximum of the $\mathrm{Re}\widehat{Z}_{11e}$ module, as well as the values of $\mathrm{Re}\widehat{Z}_{11e}$, $\mathrm{Im}\widehat{Z}_{11e}$, the phase angle $\varphi(f)$, the group delay time $\tau(f)$, and the Smith diagram. All these parameters quite fully allowed to evaluate HBAR's resonant processes both in a qualitatively and quantitatively sense in the frequency range from 0.6 up to 20 GHz together with a temperature change within 4–400 K.

To determine an absolute value of the BAW phase velocity in the substrate, two different methods were used. Common to both methods was that the antiresonance frequencies $f_{a,n}$, determined about the maxima of $\mathrm{Re}\widehat{Z}_{11e}$ module, were measured in the vicinity of an odd half-wave resonance of the thin-film piezoelectric transducer, for example, designated as $f_{p,k}$. The reason was that the near such frequency, within the substrate thickness approximately an integer $(n-1)$ of half-waves, should be fitted at HBAR's excitation on antiresonance points $f_{a,n}$. In this case, the HBAR's quality factor tends to a maximum value. The phase velocity in the substrate V in accordance with the first approach can be calculated by the formula

$$V = \frac{2df_{a,n}}{n-k}, \tag{16}$$

where d is the substrate's thickness and $k = 1, 3, 5, \ldots$ is the number of the TFPT half-wave resonance. But an accuracy of the determination of the phase velocity was strongly depended on the correct definition of an overtone number n in the vicinity of the frequency $f_{p,k}$. In the real experiment, it was far from always possible to track all antiresonances, especially in the low-frequency band and bands with high ultrasonic attenuation. In the HBARs investigated, the value of n could reach the values of 200–300 or more, which also made difficult an accurate determination of n.

The second method determining the phase velocity in a substrate was based on the relation obtained taking into account the results (Ref. [17]) about the relation for $\Delta f(N)$ of the upper limit of the spacing between parallel resonant frequencies (SPRF):

$$V \cong 2d\Delta f(N)\left(1 + \frac{\rho_{\mathrm{AlN}}h_{\mathrm{AlN}} + \rho_{\mathrm{Al}}h_{\mathrm{Al}} + \rho_{\mathrm{Mo}}h_{\mathrm{Mo}}}{\rho_{\mathrm{Diam}}}\right), \tag{17}$$

where the corresponding density and thickness of layers or substrate should be inserted in accordance with the order in the "Al/(001) AlN/Mo/(100) diamond" PLS (see **Figure 7a**). In practice, a quantity $\Delta f(N) = f_{a,n+1} - f_{a,n}$ should be chosen in the frequency band called N-region where the maximal Q_n magnitude for nth acoustic overtone of HBAR was measured.

6. Microwave acoustic properties of diamond-based HBARs and SAW resonators utilizing aluminum nitride and aluminum-scandium nitride piezoelectric films

Detailed study of microwave acoustic properties of diamond-based HBARs realized by aluminum nitride and aluminum-scandium nitride piezoelectric films has been fulfilled by a set of

Sample	Piezoelectric layered structure	Thickness (in microns) of			
		Diamond substrate	Piezoelectric film	Top electrode	Bottom electrode
1	Al/(001) AlN/Mo/(100) diamond	299	1.04	0.200	0.150
2	Al/(001) ASN/Mo/(100) diamond	488	1.125	0.140	0.160
3	Al/(001) ASN/Mo/(100) diamond	501	1.125	0.140	0.160
4	Al/(001) AlN/Mo/(100) diamond	180	2.790	0.107	0.135
5	Al/(001) AlN/Mo/(111) diamond	497	2.790	0.107	0.135
6	Al/(001) AlN/Mo/(110) diamond	1274	2.790	0.107	0.135
7	Al/(001) AlN/Mo/(100) diamond	482	0.970	0.105	0.176
8	Al/(001) AlN/Mo/(100) diamond	1107	0.970	0.105	0.176
9	Al IDT/(001) AlN/(001)[110] diamond SAW resonator, d = 10 microns	516	2.790	0.114	—

Table 1. DUT samples based on AlN and ASN piezoelectric layered structures.

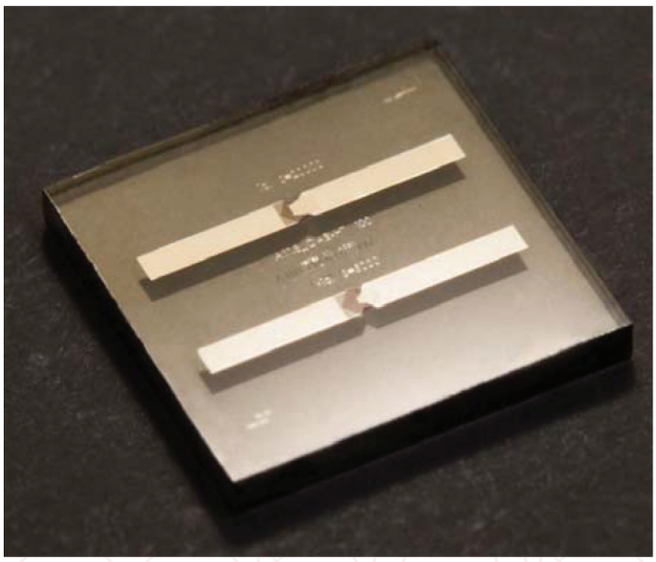

Figure 10. The view of the HBAR's sample 3 based on PLS "Al/(001) ASN/Mo/(100) diamond".

samples 1, 2, and 3 (**Table 1**). For example, in **Figure 10** one can see the view of the HBAR's sample 3 based on PLS "Al/(001) ASN/Mo/(100) diamond." On the diamond substrate, two independent HBARs designated as 1a and 1b and differing the effective resonant areas as 20,000 and 5000 square microns, respectively, are located. Topology of the top and bottom electrodes was especially developed to be convenient for an investigation of temperature dependences of HBAR's acoustic parameters within a wide range from 4 up to 400 K.

Results on microwave quality factor Q and effective electromechanical coupling coefficient (EMCC) of diamond-based HBARs (samples 1 and 3) are presented in **Figures 11** and **12**. As one can see from **Figures 11a** or **12a**, the frequency dependence of HBAR's quality factor Q

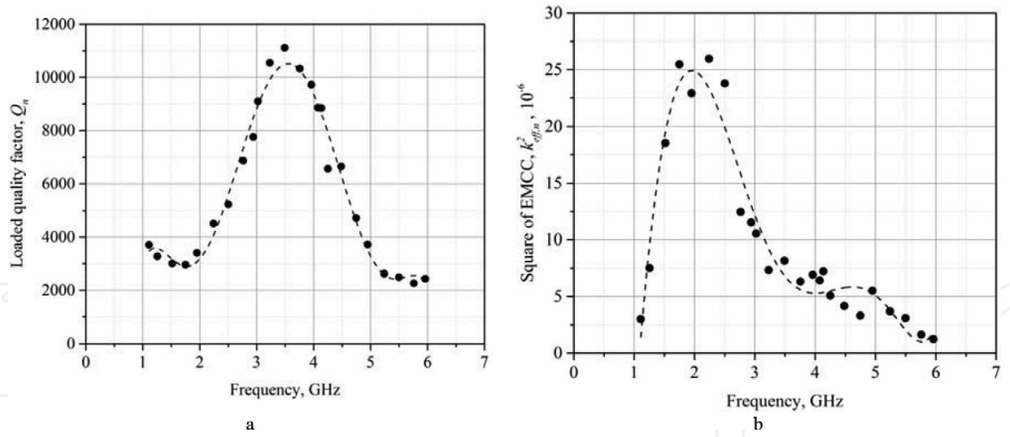

Figure 11. Frequency dependencies of quality factor (a) and the square of EMCC (b) obtained for sample 1 (PLS Al/(001) AlN/Mo/(100) diamond).

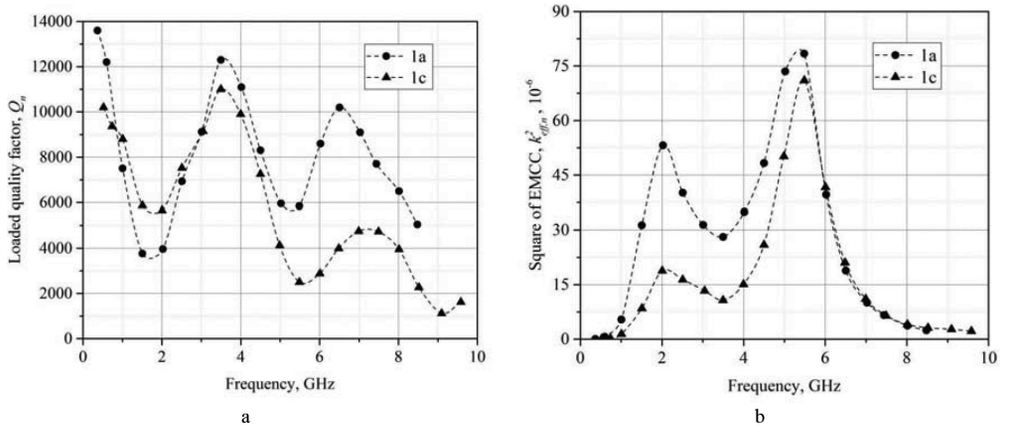

Figure 12. Frequency dependencies of quality factor (a) and the square of the EMCC (b) obtained for sample 3 (PLS Al/(001) ASN/Mo/(100) diamond).

demonstrates a typical behavior observed in piezoelectric layered structures, and such peculiarities as maximal and minimal Q magnitudes at the several frequency bands can be explained by the coinciding of an operational frequency and TFPT eigenfrequencies. Briefly speaking, maximal and minimal Q magnitudes are obtained when the quantities $k\lambda/2$ or $k\lambda/4$ are approximately equal to the TFPT thickness, respectively, and k = 1, 3, 5, …, and λ is the acoustic wave length. For more details see the paper [18].

In order to calculate the square of EMCC, $k^2_{\text{eff},\,n}$, at a given frequency $\omega_{p,n}$ of parallel resonance of nth acoustic overtone, first the loss resistance R_n was calculated from experimentally obtained impedance Z_{11e} by the relation $R_n = \text{Re}Z_{11e}$. Taking into account the Q_n factor measured for nth acoustic overtone, one can obtain the square of EMCC by the equation taken from Ref. [6]:

$$k^2_{\text{eff},\,n} = \frac{\omega_{p,\,n} C_0 R_n}{Q_n}, \tag{18}$$

where C_0 is the TFPT static capacitance.

Then, close to the frequency of the first half-wave resonance of TFPT called *N*-region according to [16], the value of $n(N)$ for an acoustic overtone with maximal Q_n factor was determined, and the calculation of $k^2_{\text{eff},\,n}(N)$ was carried out using the formula.

$$k^2_{\text{eff},\,n}(N) = \frac{\omega_{p,\,n(N)} C_0 R_{n(N)}}{Q_{n(N)}}. \tag{19}$$

It is interesting to compare the AlN and ASN piezoelectric properties taking into account such electromechanical coupling coefficient as the k_t quantity which is defined for the thickness-extensional mode of a conventional piezoelectric resonator and can be calculated taking into account the piezoelectric, elastic, and dielectric properties of a piezoelectric material:

$$k_t^2 = \frac{e_{33}}{C_{33}^E \varepsilon_{33}^S}, \tag{20}$$

where e_{33}, C_{33}^E, and ε_{33}^S are the piezoelectric, dielectric, and elastic constants, respectively. The second and last ones should be measured at the constant electric field and at the constant strain conditions, respectively.

Following to [16], the relation between k_t^2 and $k^2_{\text{eff},\,n}(N)$ can be written in the form.

$$k_t^2(N) \cong \frac{\rho_{\text{AlN}} h_{\text{AlN}} (\rho_{\text{AlN}} h_{\text{AlN}} + \rho_{\text{Al}} h_{\text{Al}} + \rho_{\text{Mo}} h_{\text{Mo}} + \rho_{\text{Diam}} h_{\text{Diam}})}{(\rho_{\text{AlN}} h_{\text{AlN}} + \rho_{\text{Al}} h_{\text{Al}} + 0.5\rho_{\text{Mo}} h_{\text{Mo}})^2} k^2_{eff,\,n}(N) \tag{21}$$

where the corresponding density and thickness of layers or substrate are the same as in Eq. (21). Data on k_t^2 values obtained for the samples 1–3 were summarized in **Table 2**. For of true comparison of results, the samples with the close dimensions and shape of TFPT have to be chosen. So, the samples 1 and 2 based on ASN piezoelectric film were obtained in the same process. Then, the overtones with close resonant frequencies have been selected. Note that studied HBARs based on PLSs differing the material of piezoelectric films and substrate thickness demonstrate the close magnitudes of quality factor Q ~ 11,000–12,000 which corresponds to comparatively high-quality parameter $Q{\cdot}f \sim 4.2{\cdot}10^{13}$ Hz at 3500 MHz.

As a main result, one can emphasize that the application of aluminum-scandium nitride as piezoelectric material leads to a drastic increase of both the effective $k^2_{\text{eff},\,n}$ and k_t^2 EMCCs up to 2.5 times. Other things being equal, the ASN-based acoustoelectronic devices will have the prospective advantages.

Sample	PLS	Frequency (MHz)	$k^2_{\text{eff},\,n}(N)$, 10^{-5}	k_t^2, 10^{-3}	k_t (%)
1	Al/(001) AlN/Mo/(100) diamond	3550	0.82	1.34	3.7
2	Al/(001) ASN/Mo/(100) diamond	3500	3.0	8.85	9.4
3	Al/(001) ASN/Mo/(100) diamond	3500	2.81	7.82	8.8

Table 2. Data on EMCCs of the HBAR samples investigated.

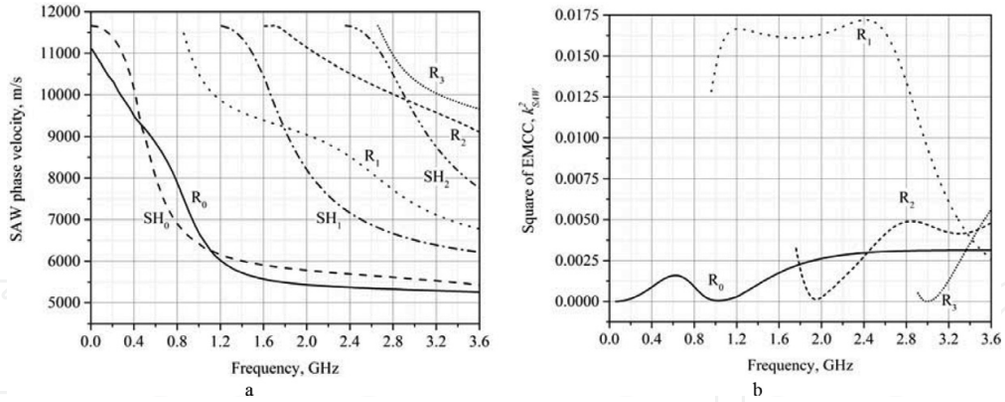

Figure 13. Frequency dependencies of SAW phase velocities (a) and the square of the EMCC (b) calculated for sample 9 (PLS "Al IDT/(001) AlN/(001)[110] diamond"). Curves designated as R_0, R_1, R_2, … and SH_0, SH_1, SH_2, … should be associated with Rayleigh or surface horizontal-type waves, respectively.

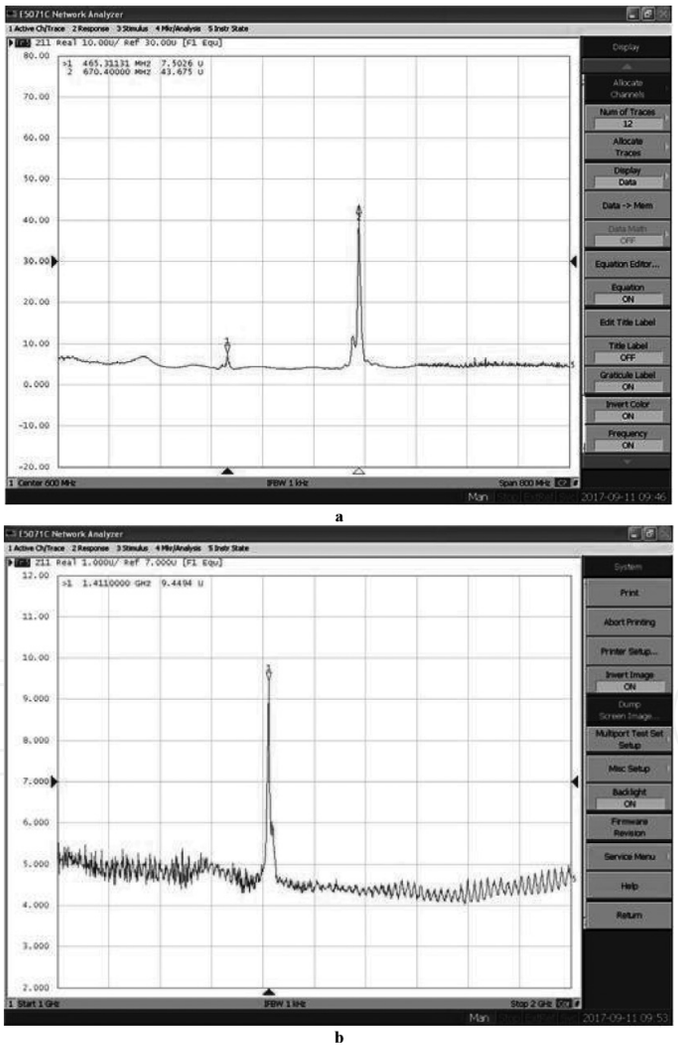

Figure 14. Amplitude and frequency characteristics of DUT sample 9 based on PLS "Al IDT/(001) AlN/(001)[110] diamond" at room temperature: (a) impedance Z_{11} in the frequency band 400–600 MHz and (b) impedance Z_{11} in the vicinity of 1400 MHz. The number of MSR electrode pairs was equal to $N = 32$.

As a DUT sample 9 (see **Table 1**), the SAW resonator based on PLS "Al IDT/(001) AlN/(001) [110] diamond" was investigated in the frequency band from 400 up to 1500 MHz at the SAW propagation in the [110] direction on the (001) crystalline cut of diamond. Scheme of a single-port SAW resonator was presented in **Figure 7b**. Distance between the nearest electrodes of IDT and MSR was taken as d = 10 microns at the width of an electrode as 5 microns. The number of MSR electrode pairs was varied from N = 16 up to 128. Because the SAW propagation was studied in the piezoelectric layered structure, the last one should be considered as a thin-film waveguide. In this case the dispersion of SAW phase velocities as well as other parameters must be taken into account. As an example such dispersion dependences of SAW phase velocities and EMCC were calculated for the PLS considered (**Figure 13**).

The square of the EMCC concerned with surface acoustic waves was calculated by a conventional relation as.

$$k^2_{\mathrm{SAW}} = 2\frac{V_{\mathrm{SAW}} - V_{\mathrm{SAW},s}}{V_{\mathrm{SAW}}}, \tag{22}$$

where V_{SAW} and $V_{\mathrm{SAW},s}$ should be defined at a free or shorted surface boundary conditions. In the last one, a conductive layer with an infinitesimal thickness should cover the surface of a piezoelectric crystal. Analyzing **Figure 13b**, one can conclude that the waves of surface horizontal type cannot be excited at a given orientation of piezoelectric film. But the Rayleigh-type waves could be excited at some frequency bands distinctive for waves of the different orders. Note that the EMCC of the R_1 mode, so-called Sezawa wave, should have a considerably more value than that in conventional Rayleigh mode R_0. Experimental data obtained by sample 9 are presented in **Figure 14**. Resonance frequencies of the SAW modes were detected as 465, 672, and 1412 MHz. Taking into account the data in **Figure 14**, one can define the type of SAW

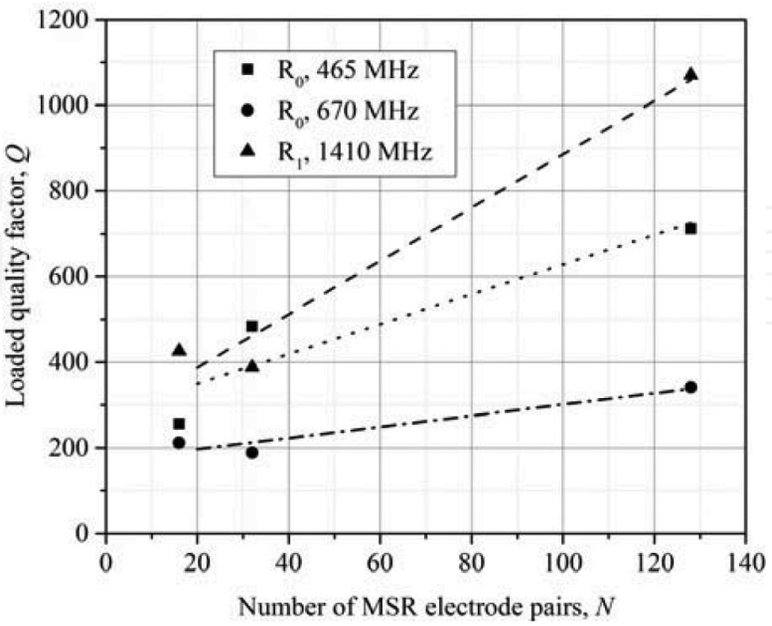

Figure 15. Dependence of the quality factor of SAW resonators in the of DUT sample 9 on the number of MSR electrode pairs for three SAW modes (PLS "Al IDT/(001) AlN/(001)[110] diamond").

http://dx.doi.org/10.5772/intechopen.76715

modes as the first (465 MHz) and second (672 MHz) harmonics of R_0 mode and the third harmonics of R_1 mode (1412 MHz). It was obtained that the quality factor of SAW resonators was strongly depended on the number of MSR electrode pairs (**Figure 15**). This corresponds to lower-energy losses in SAW resonator and a decrease in the passband of the frequency response. The highest $Q \approx 1050$ was observed for the R_1 Sezawa mode at the resonant frequency 1412 MHz.

7. Investigation of temperature dependences of acoustic parameters in diamond-based piezoelectric layered structures

In a way described in **Section 5,** temperature dependences of the loaded quality factor Q_n for a lot of acoustic overtones and the phase velocity V of longitudinal acoustic wave in the [100] direction of synthetic IIa type diamond are shown in **Figure 16**. As a DUT the HBAR sample 4 based on the piezoelectric structure "Al/AlN/Mo/(100) diamond" (see **Table 1**) was chosen. For this sample, the measurements were performed at the operating frequency of 5.41 GHz. Value of the phase velocity V = 17,542 m/s obtained at room temperature coincides with that measured earlier using the pulse-phase method operating on the frequencies of 10–200 MHz [18]. When calculating the temperature dependence of both the phase velocity and elastic modulus, the change in the thickness and density of a diamond substrate due to linear thermal expansion was taken into account by the data in Ref. [19]. In that case, the temperature dependence of an elastic modulus C_{11} of diamond was calculated in accordance with the relation.

$$C_{11}(T) = \rho(T)[V(T)]^2, \tag{23}$$

where in those calculations the diamond's density at room temperature ρ= 3516 kg/m^3 was taken, and $V(T)$ was the calculating value of the phase velocity of longitudinal acoustic wave propagating along the in [100] crystalline direction of diamond at a given temperature. First-order temperature coefficient of the BAW velocity was evaluated as $5.1 \cdot 10^{-6}$ K^{-1} in the vicinity of a room temperature. Comparison of our data on the temperature dependence of diamond's

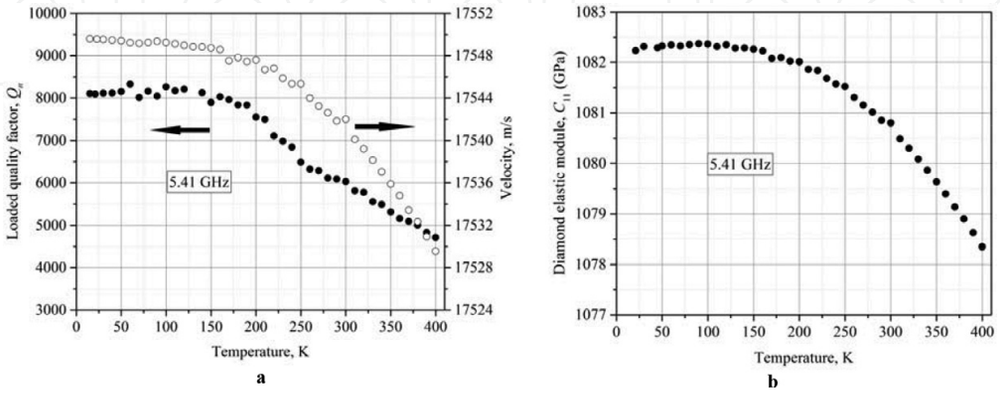

Figure 16. Temperature dependences of a loaded Q-factor and BAW phase velocity in the direction [100] of synthetic diamond (a) and the C_{11} elastic modulus of diamond (b) obtained by sample 4.

elastic modulus C_{11} obtained in the temperature range 10–303 K, with the corresponding one in Ref. [20] measured at an operational frequency of up to 60 MHz in the temperature range 77–323 K, has shown a good qualitative agreement. Some quantitative difference can be, firstly, due to the distinction in the objects of research, since we have used the samples based on the IIa type synthetic diamond, and in Ref. [20] a natural diamond has been investigated, and, secondly, with the fact that the value of diamond density 3516 kg/m^3 in our calculations has been differed from 3512 kg/m^3 which was used in Ref. [20].

Qualitatively, the temperature changes in the elastic modulus correspond to the conventional variation of elastic properties in a lot of solid states. One can emphasize on the existence of two temperature regions at which a clearly distinctive behavior of elastic properties as well as quality factor was observed: firstly, a weak dependence in the low-temperature region, which corresponds to the "freezing out" of the acoustic phonons and, secondly, a well-formed dependence close to linearly proportional one in the relatively high-temperature region, where, according to Planck's law, a lot of acoustic phonons will be excited (**Figure 16)**. Note that the temperature dependences of the elastic moduli at higher temperatures are related to the lattice anharmonicity: if the temperature is raised, the effective lattice stiffness decreases by increasing the distance between ions participating in the lattice vibrations. This ultimately leads to a nonlinear interaction between the phonons.

Research of the temperature dependence of HBAR parameters was performed with using a set of samples which were different in crystallographic orientations of diamond substrate, a thickness of films of aluminum nitride and aluminum-scandium nitride, an electrode topology, etc. The choice of a given piezoelectric film thickness was mainly associated with the TFPT peculiarities: if it is desirable to get a more TFPT effectiveness at low frequencies, it should necessarily deposit a higher thickness. So, in a way to obtain the results at the frequency band below 1 GHz, the appropriate TFPTs were based on AlN films with the thickness up to 2.79 microns (see **Table 1**, samples 4–6). Besides it, the choice of an operational frequency should be agreed with the frequency bands where the maximal *Q*-factor will be observed (see **Section 6**). All the results (**Figure 17**) on the temperature dependences of a loaded quality factor $Q(T, f)$ in a region from 10 up to 400 K at different frequencies from 0.8 up to 4.9 GHz were obtained by the samples 3–8 based on the (100), (110), and (111) diamond substrates (see **Table 1)**.

In **Figure 17a** the normalized magnitudes of *Q*-factor have been presented when the reference $Q_{400\ K}$ values were taken at the point 400 K, and the absolute *Q* values were displayed in **Figure 17b** and **c**.

It should be emphasized that an evident general conclusion, such as the results obtained at relatively low frequencies below 1.1 GHz, was quite different in comparison with ones measured at the frequencies up to 5 GHz. Such behavior was observed for all the samples regardless the substrate's orientation. Really, observing the *Q*-factor variation under the temperature decrease, one can see a considerable increasing *Q* value with further achievement of a maximal magnitude at low temperatures, when the high-frequency acoustic overtones were taken into account. On the other hand, the *Q*-factor of overtones excited on the frequencies below 1.1 GHz had only a monotonic temperature dependence as a slightly *Q* increasing at low temperatures. We assume that the difference could be explained in terms of changing

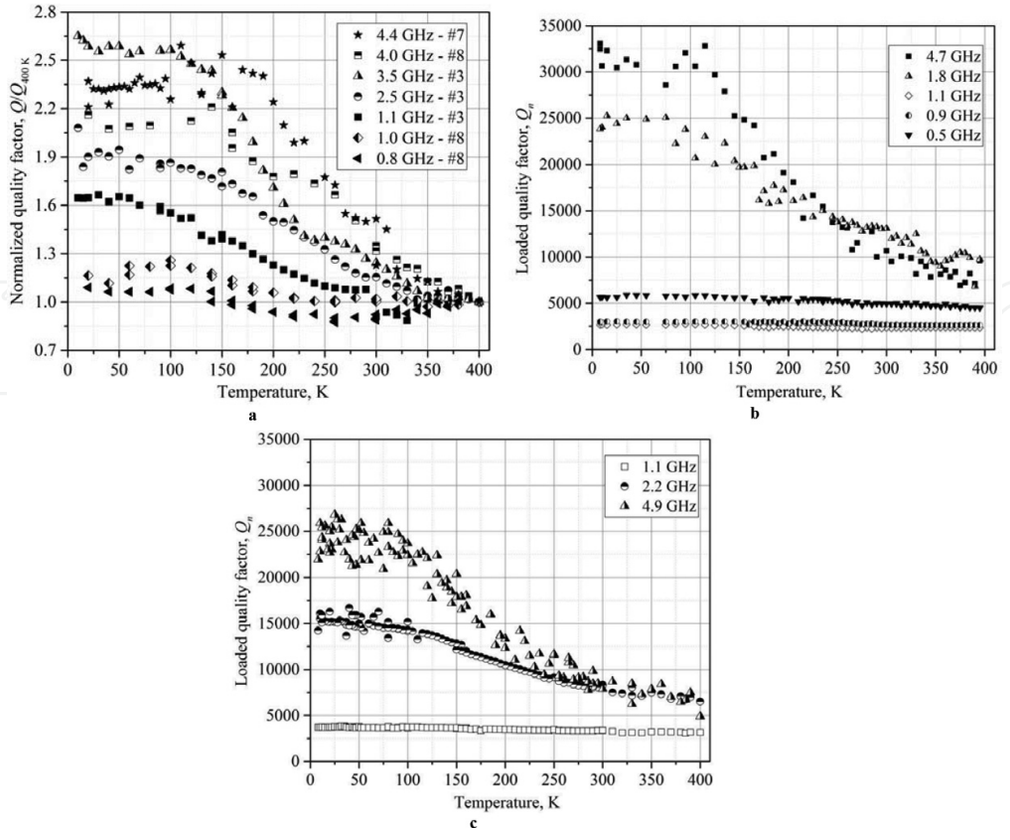

Figure 17. Temperature and frequency dependences of a normalized loaded *Q*-factor in the HBAR's samples 3, 7, and 8 with the propagation of microwave longitudinal waves along the [100] diamond's direction (a); temperature and frequency dependences of the quality factor Q_n in the HBAR's sample 6 with the propagation of microwave longitudinal waves along the [110] diamond's crystalline direction (b); temperature and frequency dependences of the quality factor Q_n in the HBAR's sample 5 with the propagation of microwave longitudinal waves along the [111] diamond's crystalline direction (c).

mechanism of acoustic attenuation from Akhiezer's type at the frequencies below 1.1 GHz to Landau-Rumer's one at a higher frequency band in the single-crystalline diamond. In the last one, if taking a given point close to room temperature, the so-called quality parameter $Q \cdot f$ with the frequency variation must change as a linearly proportional function in a manner of $Q \cdot f \sim f$, i.e., the quality factor must not depend on the frequency (Ref. [21]) in that approximation. Earlier, we have obtained by means of HBAR based on PLS involved the single-crystalline diamond substrate and AlN thin-film piezoelectric transducer that such assumption has been quite fulfilled for operational frequencies up to 20 GHz at room temperature (Ref. [7]). Also, this fact is of great practical importance, as it allows realizing acoustoelectronic devices on diamond substrates at hypersonic frequencies with an acceptable level of acoustic attenuation.

8. Conclusion

Theory of the influence of an external loading on the acoustic parameters of piezoelectric five-layered structure as "Al/(001) AlN/Mo/(001) diamond/Me" has been derived. Approach how to

obtain the boundary conditions can be spread on the more complicated multilayered structures too. On the base of that theory, the own software "Modeling of the processes of resonant acoustic spectroscopy in multilayered structures" has been developed. Study of the influence of metal film deposition as the fifth layer on the change of the overtone resonant frequency of diamond-based PLS "Al/(001) AlN/Mo/(001) diamond/Me" (Me = Al, Mo) has been fulfilled. It has been obtained that metal film deposition leads to the decrease of resonant frequency with the thickness increasing both the metals.

HBAR based on the PLS "Al/(001) AlN/Mo/(001) diamond" has been investigated in terms of 3D FEM simulation by the software COMSOL Multiphysics. Boundary conditions on the top and bottom surfaces of a model sample were chosen as the free ones, and on all the vertical surfaces as the symmetrical ones. All the dimensions of a model sample were close to appropriate ones in the experimental sample. Besides Lamb waves the BAW and SAW modes of Rayleigh and SH type were found. It has been shown that the calculated data on HBAR's resonant frequency in 2D approximation were in close accordance with the similar obtained in 3D approximation. Elastic displacement patterns arising for the SH-type waves in the PLS "Al/(001) AlN/Mo/(001) diamond" were obtained in 3D image. Dispersive dependences of SH-type wave velocities on a frequency for a number of the first dispersive SH-branches have been calculated. Comparison of the data obtained by 3D FEM simulation with the theory and 2D FEM results has been demonstrated a good agreement between a model and theory. Visualization of elastic displacement fields associated with the SAW of Rayleigh type has been realized, and calculated phase velocity of the SAW propagating in a given direction on the (001) diamond surface was quite the same as known data.

Peculiarities of the technology of aluminum nitride and aluminum-scandium nitride piezoelectric films have been discussed. The $Al_{0.8}Sc_{0.2}N$ composition was obtained to create the microwave BAW and SAW test devices as diamond-based HBAR and SAW resonator. By the X-ray diffraction pattern, it has been proven that the crystallites of ASN film had a preferred orientation (00·2) and the full width at half maximum for that reflection was 0.24°. This shows on a good quality texture of axial type along the sixfold axis of the wurtzite-type structure. Data obtained will be used for the future development of ASN film technology in a way of producing a number of compositions with the better piezoelectric properties.

Detailed study of microwave acoustic properties of diamond-based HBARs realized by aluminum nitride and aluminum-scandium nitride piezoelectric films has been fulfilled by a set of the samples. Topology of the top and bottom electrodes as well as piezoelectric film areas was especially developed to be convenient for an investigation of temperature dependences of HBAR's acoustic parameters within a wide range from 4 up to 400 K. Investigated HBARs based on PLSs differing the material of piezoelectric films and substrate thickness have demonstrated the close magnitudes of quality factor Q ~ 11,000–12,000 which corresponded to comparatively high-quality parameter $Q \cdot f \sim 4.2 \cdot 10^{13}$ Hz at 3500 MHz. As a main result, one can emphasize that the application of aluminum-scandium nitride as a piezoelectric material has resulted in a drastic increase of the effective electromechanical coupling coefficient up to

2.5 times in comparison with that in aluminum nitride. Other things being equal, the ASN-based acoustoelectronic devices will have the prospective advantages.

Single-port SAW resonator based on PLS "Al IDT/(001) AlN/(001)[110] diamond" has been investigated in the frequency band from 400 up to 1500 MHz at the SAW propagation in the [110] direction on the (001) crystalline cut of diamond. Highest $Q \approx 1050$ was observed for the Sezawa mode at the resonant frequency 1412 MHz. Note that the microwave SAW devices have demonstrated a comparatively low performance in comparison with diamond-based HBAR taken at the same operational frequency.

Method of HBAR microwave studies of temperature dependences of such acoustic properties as BAW phase velocity and quality factor in the temperature region 4–400 K and frequency band 0.5–5 GHz has been developed. A general conclusion should be emphasized that the results on the temperature dependence of diamond's *Q*-factor obtained at relatively low frequencies below 1.1 GHz were quite different in comparison with the ones measured at the frequencies up to 5 GHz. Such behavior was observed for all the samples regardless the substrate's orientation. One can assume that the difference could be explained in terms of changing mechanism of acoustic attenuation from Akhiezer's type at the frequencies below 1.1 GHz to Landau-Rumer's one at a higher frequency band in the single-crystalline diamond. In the last case, if taking a given point close to room temperature, the quality parameter $Q \cdot f$ with the frequency variation must change as a linearly proportional function in a manner of $Q \cdot f \sim f$, i.e., the quality factor must not depend on the frequency in that approximation. That result has earlier been proven for operational frequencies up to 20 GHz at room temperature [7]. Also, this fact is of great practical importance, as it allows realizing acoustoelectronic devices on diamond substrates at hypersonic frequencies with an acceptable level of acoustic attenuation.

Acknowledgements

This work was supported by a grant of the Russian Science Foundation (project 16-12-10293).

Author details

Boris P. Sorokin[1,2]*, Gennady M. Kvashnin[1], Andrey S. Novoselov[1,2], Sergey I. Burkov[3], Anton B. Shipilov[1,2], Nikolay V. Luparev[1], Victor V. Aksenenkov[1] and Vladimir D. Blank[1]

*Address all correspondence to: bpsorokin1953@yandex.ru

1 Technological Institute for Superhard and Novel Carbon Materials, Troitsk, Moscow, Russian Federation

2 Moscow Institute of Physics and Technology, Dolgoprudny, Moscow Region, Russian Federation

3 Siberian Federal University, Krasnoyarsk, Russian Federation

References

[1] Lakin KM. Thin film resonator technology. IEEE Transactions on Ultrasonics, Ferroelectrics, and Frequency Control. 2005;**52**:707-716. DOI: 10.1109/TUFFC.2005.1503959

[2] Part 4. Acoustic wave based microdevices. In: Marco G Beghi, editor. Acoustic Waves—From Microdevices to Helioseismology. Rijeka, Croatia: Intech; 2011. pp. 419-652. DOI: 10.5772/1032

[3] Akiyama M, Kamohara T, Kano K, Teshigahara A, Takeuchi Y, Kawahara N. Enhancement of piezoelectric response in scandium aluminum nitride alloy thin films prepared by dual reactive cosputtering. Advanced Materials. 2009;**21**:593-596. DOI: 10.1002/adma.200802611

[4] Zhang H, Pang W, Yu H, Kim ES. High-tone bulk acoustic resonators on sapphire, crystal quartz, fused silica, and silicon substrates. Journal of Applied Physics. 2006;**99**:124911. DOI: 10.1063/1.2209029

[5] Baumgartel L, Kim ES. Experimental optimization of electrodes for high *Q*, high frequency HBAR. In: Proceedings of 2009 IEEE Intl Ultrasonics Symp. Rome, Italy; 2009. pp. 2107-2110. DOI: 10.1109/ULTSYM.2009.5441814

[6] Mansfel'd GD, Alekseev SG, Polzikova NI. Unique properties of HBAR characteristics. In: Proceedings of the 2008 IEEE Intl Ultrasonics Symp. Beijing, China; 2008. pp. 439-442. DOI: 10.1109/ULTSYM.2008.0107

[7] Sorokin BP, Kvashnin GM, Novoselov AS, Bormashov VS, Golovanov AV, Burkov SI, Blank VD. Excitation of hypersonic acoustic waves in diamond-based piezoelectric layered structure on the microwave frequencies up to 20 GHz. Ultrasonics. 2017;**78**:162-165. DOI: 10.1016/j.ultras.2017.01.014

[8] Benetti M, Cannata D, Fabio Di Pietrantonio FD, Verona E. Growth of AlN piezoelectric film on diamond for high-frequency surface acoustic wave devices. IEEE Transactions on Ultrasonics, Ferroelectrics, and Frequency Control. 2005;**52**:1806-1811. DOI: 10.1109/TUFFC.2005.1561635

[9] Fujii S, Kawano S, Umeda T, Fujioka M, Yoda M. Development of a 6 GHz resonator by using an AlN Diamond structure. In: Proceedings of the 2008 IEEE Intl Ultrasonics Symp. Beijing, China; 2008. pp. 1916-1919. DOI: 10.1109/ULTSYM.2008.0472

[10] Aleksandrov KS, Sorokin BP, Burkov SI. Effective Piezoelectric Crystals for Acoustoelectronics, Piezotechnics and Sensors. Vol. 1. Novosibirsk: SB RAS Publishing House; 2007. p. 501. (in Russian)

[11] Alekseev SG, Kotelyanskii IM, Polzikova NI, Mansfel'd GD. Study of layered structures using modified acoustic resonator spectroscopy. Journal of Communications Technology, Electronics. 2015;**60**:300-307. DOI: 10.1134/S1064226915030018

[12] Sorokin BP, Burkov SI. Modeling of the processes of resonant acoustic spectroscopy in multilayered structures. Certificate #2017660543 of government registration of computer software. Russian Federation; 2017

[13] Sorokin BP, Kvashnin GM, Telichko AV, Burkov SI, Blank VD. Piezoelectric layered structures based on the synthetic diamond. In: Ogawa T, editor. Piezoelectric Materials. Rijeka, Croatia: Intech; 2016. pp. 161-199. DOI: 10.5772/62630

[14] Sorokin BP, Kvashnin GM, Telichko AV, Novoselov AS, Burkov SI. Lamb waves dispersion curves for diamond based piezoelectric layered structure: Experimental investigation and computer modeling. Applied Physics Letters. 2016;**108**:113501. DOI: 10.1063/1.4943945

[15] Sorokin BP, Bormashov VS, Korostilev EV, Novoselov AS, Doronin MA, Kravchuk KS, Blank VD. Usage of electron back scattering diffraction for investigation of buried damage layer underneath a single crystalline diamond surface. Journal of Materials Science: Materials in Electronics. 2017;**28**:13464-13471. DOI: 10.1007/s10854-017-7185-y

[16] Teshigahara A, Hashimoto K, Akiyama M. Scandium aluminum nitride: Highly piezoelectric thin film for RF SAW devices in multi GHz range. In: Proceedings of 2012 IEEE Intl Ultrasonics Symp. Dresden, Germany; 2012. pp. 1-5. DOI: 10.1109/ULTSYM.2012.0481

[17] Zhang Y, Wang Z, Cheeke JDN. Resonant spectrum method to characterize piezoelectric films in composite resonators. IEEE Transactions on Ultrasonics, Ferroelectrics, and Frequency Control. 2003;**50**:321-333. DOI: 10.1109/TUFFC.2003.1193626

[18] Sorokin BP, Kvashnin GM, Kuznetsov MS, Telichko AV, Burkov SI. Influence of the temperature and uniaxial pressure on the elastic properties of synthetic diamond single crystal. In: Proceedings of 2012 IEEE Intl Ultrasonics Symp. Dresden, Germany; 2012. pp. 763-766. DOI: 10.1109/ULTSYM.2012.0190

[19] Novikov NB, editor. Physical Properties of Diamond (in Russian). Handbook. Naukova dumka: Kyiv; 1987. p. 188

[20] McSkimin HJ, Andreatch PJ. The elastic stiffness moduli of diamond as a function of pressure and temperature. Applied Physics. 1972;**43**:2944-2949. DOI: 10.1063/1.1661636

[21] Tabrizian R, Rais-Zadeh M, Ayazi F. Effect of phonon interactions on limiting the *f*·*Q* product of micromechanical resonators. In: Proceedings of 15 Intl Conf on Solid-State Structures, Actuators and Microsyst. Denver, USA; 2009. pp. 2131-2134. DOI: 10.1109/SENSOR.2009.5285627

IntechOpen